PCCP

COMMUNICATION

View Article Online
View Journal | View Issue

Cite this: *Phys. Chem. Chem. Phys.*, 2015, **17**, 8614

Received 29th January 2015,
Accepted 2nd March 2015

DOI: 10.1039/c5cp00583c

www.rsc.org/pccp

Enantioselective femtosecond laser photoionization spectrometry of limonene using photoelectron circular dichroism

Mohammad M. Rafiee Fanood,[a] Maurice H. M. Janssen[a] and Ivan Powis*[b]

Limonene is ionized by circularly polarized 420 nm femtosecond laser pulses. Ion mass and photoelectron energy spectra identify the dominant (2 + 1) multiphoton ionization mechanism, aided by TDDFT calculations of the Rydberg excitations. Photoelectron circular dichroism measurements on pure enantiomers reveal a chiral asymmetry of ±4 %.

Terpenes are one of the most important and abundant classes of natural products. The occurrence of chiral terpenes is known to show enantiomeric variation between species, but recent studies have revealed enantiomeric variations in biogenic emissions within a single species,[1,2] and these differences may be linked, for example, to stress conditions experienced by the plant.[3] Monitoring enantiomer variations may thus provide key indicators of the responses of crops, forests, and even the marine ecosphere,[4] to environmental stresses such as climate change.

Limonene ($C_{10}H_{16}$– see Fig. 1 inset) is a frequently encountered exemplar of the chiral monoterpenes. Like many other terpenoids, its enantiomers are perceived to have different odours (*R*(+)-limonene: citrus fruit; *S*(−)-limonene: pine/turpentine), and in the biosphere such enantiomeric variations may be significant in signalling to populations of predators and/or pollinators. The *R*(+) enantiomer (D-limonene) finds widespread domestic uses as an odorant in food, cosmetics, and cleaning products. As a common component of biogenic volatile organic compound emissions (BVOCs), it can be expected to play a significant role in certain atmospheric processes. There is, therefore, an interest in understanding the UV photochemistry and photophysics of gaseous limonene.

In this context it is interesting to consider the potential of two more recently introduced methods for enantioselective detection and probing, both based upon laser photoionization. Loge and Boesl[5] have reported the resonant two photon ionization yield of *S*-limonene at 213 nm laser wavelength (equivalent photon energy of 5.82 eV). This excitation lies in the red foot of the limonene absorption spectrum and the circular dichroism (CD) detected in the parent ion yield has a similar asymmetry factor ($\sim 1.6 \times 10^{-3}$) to that seen in the absorption CD at the same wavelength.[6] In the present work we wish to evaluate the potential of an alternative new technique, photoelectron circular dichroism (PECD) using resonant ionization with an ultrafast laser.[7] PECD detects a forward–backward asymmetry in the photoelectron angular distribution relative to the photon beam propagation direction with asymmetry factors that range, for single photon ionization in the VUV and SXR regions, from 0.01–0.4.[8–10] Very recently it has been shown that similar asymmetries can be seen using 400 nm fs laser pulses to ionize various bicyclic monoterpenoids[11–13] or methyl oxirane,[14] although very different behaviour in the higher odd Legendre moments – uniquely accessed by the multiphoton excitation – were apparent. Here we seek further insight with a different molecular system.

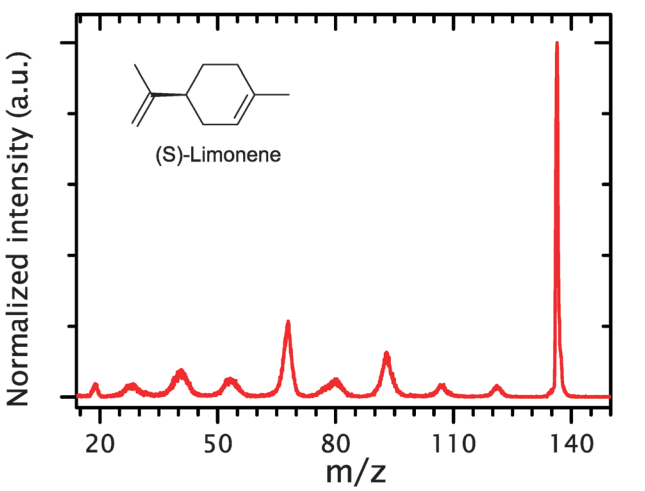

Fig. 1 Mass spectrum of *S*-limonene seeded in 0.1 bar Ne after ionization by 420 nm 150 fs laser. The parent ion is *m*/*z* 136.

[a] *LaserLaB Amsterdam, VU University Amsterdam, De Boelelaan 1081, 1081 HV Amsterdam, The Netherlands*
[b] *School of Chemistry, University of Nottingham, Nottingham NG7 2RD, UK. E-mail: ivan.powis@nottingham.ac.uk; Fax: +44 (0)115 9513562; Tel: +44 (0)115 9513467*

The experiment uses a single detector spectrometer having velocity map imaging charged particle optics for both electron and ion detection.[15] The position sensitive delay line detector[16,17] is capable of measuring the full 3D electron momentum from the time and position of arrival of individual electrons. Alternatively, by reversal of the apparatus extraction and detector potentials the time-of-flight of ions can be measured on the same detector. Because of the much longer flight times of the ions these voltages can be rapidly switched to ion mode immediately after electron detection, allowing the delayed coincidence between an electron and ion pair from a single molecular ionization event to be detected. Electrons can then be mass-tagged according to the identity of coincident ion.

A doubly skimmed, seeded molecular beam of limonene enantiomer samples (obtained from Sigma Aldrich and used without further purification) was produced after passing Ne gas (0.1 bar backing pressure) through an external stainless steel bubbler maintained at room temperature. The output of a 3 kHz repetition rate laser (Spectra Physics) was frequency doubled in a BBO crystal providing of $\sim$20 μJ, 150 fs pulses at 420 nm, loosely focussed into the molecular beam. Circular polarization was obtained with a $\lambda/4$ waveplate and was switched between left- (LCP) and right- (RCP) circular polarization every 500 s. Stokes parameters were determined by polarimetry measurements,[12] confirming a high degree of circular polarization ($|S_3| \geq 0.975$). Measurements on *R*- and *S*-enantiomers were accumulated during 49.5 and 45 million laser shots respectively and the average number of electron events per laser shots in both measurements was maintained at 0.085 to minimise false coincidences. For each enantiomer the accumulated counts were reduced to the number released into the forward (*F*) and backward (*B*) hemispheres, combining the LCP and RCP data in such a way that any residual forward–backward instrumental asymmetry (which is independent of polarization) is cancelled.[12,14] Then, the PECD asymmetry is conveniently expressed as

$$G = 4\left(\frac{F-B}{F+B}\right) \quad (1)$$

Fig. 1 shows a ToF mass spectrum which was the same for either polarization and both enantiomers. While the parent ion mass is the dominant species there is a range of smaller daughter ions present. The adiabatic ionization potential of limonene, 8.521 eV, is well established[6,18,19] and so ionization requires three 420 nm photons (equivalent energy 8.86 eV). This leaves a maximum excess energy of 0.34 eV available for the photoelectrons. On the other hand, VUV ionization at 9 eV produces negligible fragmentation[18] suggesting that there may be partial uptake of at least a fourth photon by some of the fragmentation channels observed here.

Fig. 2 shows the photoelectron kinetic energy distributions derived from the 3D electron momenta for all detected electrons, and for electrons coincident with selected parent and fragment ion masses. Again these results do not vary with either polarization or enantiomer. These photoelectron spectra are essentially identical to one another, suggesting a common ionization path for both parent and fragment ions, although the fragment ion-tagged

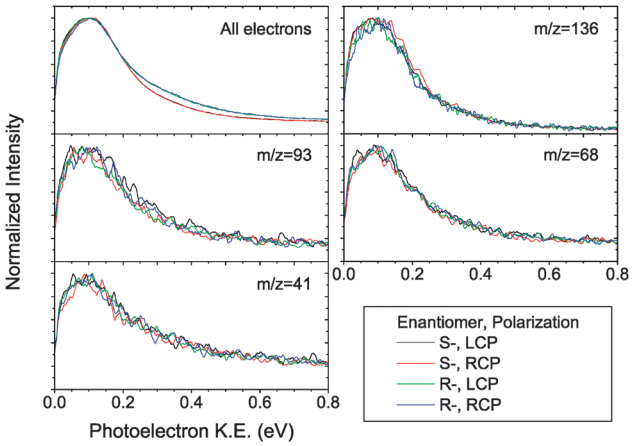

Fig. 2 Photoelectron kinetic energy distributions of limonene measured at 420 nm for all-, and for mass-tagged-electrons, as indicated.

spectra do tail slightly more to high energy suggesting that a small subset of the fragmentation may arise from more energetic ionization processes. The range of kinetic energy observed is nevertheless broadly consistent with a net three photon ionization, although the peak in the distribution is significantly below the 0.34 eV expected at the adiabatic ionization limit. Before further assigning the dominant ionization process we consider the assignment of the resonant intermediate state accessed in our experiments.

The UV absorption, and corresponding circular dichroism (CD) of limonene vapour in the range 225–150 nm was first reported by Brint *et al.*[6] (see Fig. 3). Subsequently, the absorption spectrum has been re-measured at slightly higher resolution and extended down to $\sim$120 nm.[19] Above 200 nm the absorption spectrum displays a weak pedestal, albeit with a few broad structures. Brint *et al.* assigned the first feature, at 218 nm

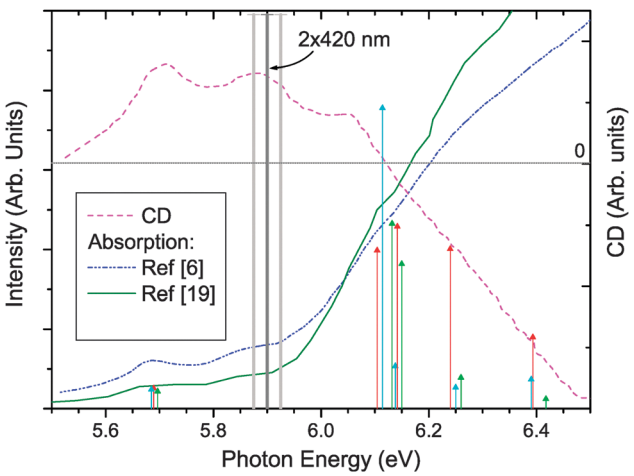

Fig. 3 UV CD[6] and absorption[6,19] spectra of limonene vapour, arbitrarily scaled to facilitate comparison. CAM-B3LYP/dAug-cc-pVDZ calculated Rydberg excitations for conformers Eq-1 (red), Eq-2 (green) and Eq-3 (cyan) are plotted offset with heights proportional to their oscillator strength. The two photon energy equivalent of the 420 nm fs laser excitation (5.9 eV) is marked, with grey bands indicating the two photon excitation range (derived from the measured laser bandwidth FWHM of 2.55 nm[14]).

(5.69 eV), to excitation from the 2π HOMO, located at the C=C double bond in the cylcohexene ring. The assignment of the upper level as the 3s Rydberg state was based upon the observed 22 915 cm^{-1} term value of this excitation.[6] A second weak feature at 210 nm (5.90 eV), also clearly visible in the CD spectrum, was assigned to the same electronic transition with one quantum of vibrational excitation, probably in the ring C=C stretching mode. A third feature at 204.9 nm (6.051 eV), this more prominent in the CD spectrum, was tentatively assigned as being the same excitation but having two quanta in this C=C stretching mode.

On the other hand, making use of the high level EOM-CCSD method and a cc-pVDZ basis with additional molecule-centred diffuse functions, Smialek *et al.*[19] calculated that excitations to the 3s and higher Rydberg series occur at somewhat higher energies, starting with the 2π → 3s transition at 6 eV. Additionally, they calculate transitions from the second highest 1π molecular orbital (located at the isopropenyl double bond) to n = 3 Rydberg series starting at 6.39 eV. However, accepting these suggested excitation energies leaves unaddressed a question concerning the identity of the absorptions in the pedestal region below 6 eV.

The assignment offered by Brint *et al.*[6] would suggest that our current choice of 420 nm wavelength is two photon resonant (equivalent energy of 5.90 eV) with the 2π → 3s (v = 1) excitation feature seen in both absorption and CD spectra (see Fig. 3). The inferred energy of the excited vibrational mode is ∼1500 cm^{-1} (0.186 eV). In the $2\pi^{-1}$ cation ground state, the principal vibrational progression observed in both threshold and He I photoelectron spectra has a first spacing of 0.174 eV and the mode has been assigned as the ring C=C stretch.[19] Assuming this is the same mode excited in the Rydberg intermediate and a Δv = 0 propensity for the Rydberg state ionization, the required ionization energy is then that for the $2\pi^{-1}$ (v^+ = 1) cation, determined as 8.695 eV from the He I photoelectron spectrum.[19] At the 420 nm three photon energy equivalent of 8.856 eV this then leaves an excess energy of just 0.16 eV. This accords reasonably well with the experimental electron energy distribution (Fig. 2) peaking at ∼0.1 eV, from which we deduce a dominant two photon resonant, three photon (2 + 1) ionization mechanism producing v^+ = 1 cation in the current experiment. This argument also tends to support the 2π → 3s (v = 1) assignment of the 5.9 eV peak. Further post-ionization photon absorption by the cation states most probably accounts for the extra fragmentation noted.

To attempt further corroboration of the spectrum assignment we have performed our own TD-DFT calculations using the long-range adjusted CAM-B3LYP and M11 functionals with a double augmented cc-pVDZ basis set at B3LYP/cc-pVDZ optimised geometries, considering the three lowest energy equatorial conformers of limonene, Eq-1, Eq-2, and Eq-3.[20] These results and previous EOM-CCSD calculations[19] are summarised in Table 1. While there is some spread in the absolute excitation energies calculated, these methods consistently indicate a ∼0.4 eV energy gap between the 2π → 3s and first 2π → 3p excitations and oscillator strengths that are approximately an order of magnitude less for the former transitions.

Guided by these observations we have plotted the CAM-B3LYP transition energies and relative oscillator strengths on Fig. 3 with an empirically chosen −0.1 eV energy offset. Although ignoring *e.g.* Franck–Condon factors the theory–experimental spectra match with this empirical adjustment is convincing. The calculated 2π → 3s excitation is brought into alignment with the 5.7 eV pedestal peak previously so assigned[6] while the steep rise in the VUV absorption spectra, and in particular a weak inflection at 6.12 eV in the higher resolution spectrum,[19] coincides with the cluster of 2π → 3p and 1π → 3s transitions. Similar results are obtained by plotting the EOM-CCSD calculations with an offset of −0.32 eV. (Systematic studies have found EOM-CCSD can overestimate excitation energies by a few tenths eV, so that this adjustment is not intrinsically surprising.[21]) Overall, we therefore favour assignment of the transitions in the pedestal region below 6 eV to the 2π → 3s electronic excitation, with higher Rydberg excitations falling above this and infer a (2 + 1) ionization mechanism at 420 nm producing vibrationally excited cations.

Table 1 Rydberg excitation energies, E, and oscillator strengths, f, calculated for limonene conformers

	EOM-CCSD ref. 19		TDDFT CAM-B3LYP/ dAug-cc-pVDZ		TDDFT M11/ dAug-cc-pVDZ	
	E (eV)	f	E (eV)	f	E (eV)	f
2π → 3s						
Eq-1	6.006	0.0027	5.790	0.0046	5.426	0.0015
Eq-2	6.013	0.0020	5.797	0.0039	5.437	0.0012
Eq-3	6.002	0.0026	5.785	0.0043	5.431	0.0013
1π → 3s						
Eq-1	6.391	0.0253	6.204	0.0358	5.844	0.0028
Eq-2	6.447	0.0118	6.250	0.0327	5.893	0.0087
Eq-3	6.435	0.0133	6.238	0.0096	5.882	0.0096
2π → 3p						
Eq-1	6.454	0.0142	6.242	0.0412	5.792	0.0304
Eq-2	6.470	0.0206	6.232	0.0419	5.815	0.0219
Eq-3	6.439	0.0247	6.214	0.0680	5.803	0.0250
2π → 3p						
Eq-1	6.540	0.0107	6.340	0.0361	5.928	0.0066
Eq-2	6.555	0.0044	6.360	0.0070	5.948	0.0023
Eq-3	6.538	0.0036	6.350	0.0048	5.929	0.0016
2π → 3p						
Eq-1	6.674	0.0026	6.493	0.0162	6.168	0.0120
Eq-2	6.761	0.0033	6.518	0.0022	6.181	0.0035
Eq-3	6.755	0.0002	6.490	0.0066	6.170	0.0014

Fig. 4 shows the multiphoton PECD asymmetry obtained for both enantiomers as a function of electron energy. The absolute magnitude is greatest in the vicinity of the peak in the electron energy distribution, and decreases on passing towards faster electrons. The *R*- and *S*-enantiomer PECD effectively mirror each other, as would be expected, an observation which also helps establish the molecular origin of the forward–backward asymmetries that are detected. Selecting a photoelectron energy of 0.0–0.2 eV that encompasses the photoelectron energy peak region we obtain asymmetry factors of −0.044 ± 0.002 for the *R*-enantiomer, and + 0.046 ± 0.002 for the *S*-enantiomer, a magnitude about 30-fold greater than the corresponding asymmetry factors previously observed in absorption[6] and ionization yield[5] measurements. There is then a decrease in the asymmetry towards higher kinetic energies which might be expected to correlate

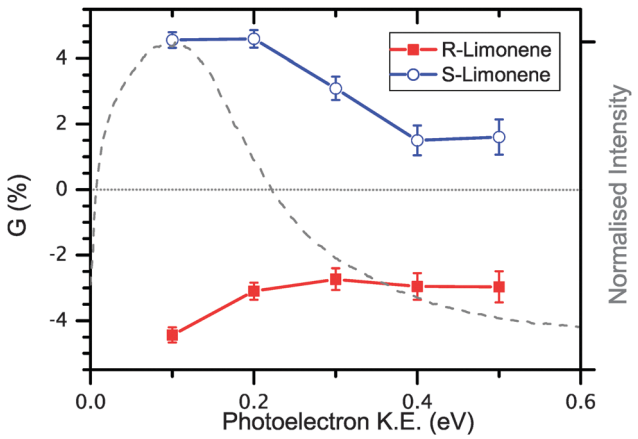

Fig. 4 420 nm multiphoton PECD asymmetry of limonene enantiomers using all electrons (no mass-tagging). Error bars are derived from Poisson count statistics. Also shown on the same energy scale as a dashed grey line is the normalised photoelectron energy distribution from Fig. 2, plotted on the same energy scale (dashed grey line, right hand axis).

with production of vibrational ground state cation, although as noted there is no distinct structure associated with this.

Conclusions

These preliminary observations of fs laser multiphoton PECD in limonene demonstrate this to be a convenient and, because of the large asymmetry factors, a potentially sensitive approach to enantiomeric identification in conjunction with laser ionization mass spectrometry. They also raise some challenges and opportunities for developing better theoretical insights. First, because of the existence of various conformers of limonene it will be necessary to develop understanding of the plausible conformer populations under experimental conditions and to account for these in computational models, since PECD is known to be exceptionally sensitive to molecular conformation. Secondly, it will be necessary to consider PECD generated not by ionization from ground state neutrals, but from excited Rydberg states, and to account for additional anisotropies introduced in the two photon excitation step. A first extension of successful single photon PECD treatments in this manner, considering the MP-PECD of camphor, provided encouraging results but much remains to be done.[12] Thirdly, according to the interpretation offered here this will be the first instance in which PECD is clearly observed from a vibrationally excited state. Recent evidence suggests that vibronic interactions with odd quanta of vibrational excitation can exert a very dramatic influence on PECD asymmetries[22,23] and such possibilities will need to be carefully checked out and validated. Further experiments using different wavelengths and excitation schemes are planned as a contribution towards tackling these challenges and opportunities.

Acknowledgements

This research was supported by the council for Chemical Sciences of the Dutch Organization for Scientific Research (NWO-CW VICI and CW-BAZIS), LASERLAB-EUROPE (European Community – Access to Research Infrastructures action of the Improving Human Potential Program, Contract no. RII-CT-2003-506350, LLAMS-1957) and the Marie Curie Initial Training Network ICONIC. Computational resources were provided by the EPSRC UK National Service for Computational Chemistry Software. Excellent technical support from Mr. R. Kortekaas is gratefully acknowledged.

Notes and references

1 W. Song, M. Staudt, I. Bourgeois and J. Williams, *Biogeosciences*, 2014, **11**, 1435–1447.
2 J. Williams, N. Yassaa, S. Bartenbach and J. Lelieveld, *Atmos. Chem. Phys.*, 2007, **7**, 973–980.
3 N. Yassaa and J. Williams, *J. Chromatogr. A*, 2007, **1141**, 138–144.
4 N. Yassaa, I. Peeken, E. Zollner, K. Bluhm, S. Arnold, D. Spracklen and J. Williams, *Environ. Chem.*, 2008, **5**, 391–401.
5 C. Loge and U. Boesl, *ChemPhysChem*, 2011, **12**, 1940–1947.
6 P. Brint, E. Meshulam and A. Gedanken, *Chem. Phys. Lett.*, 1984, **109**, 282.
7 M. H. M. Janssen and I. Powis, *Phys. Chem. Chem. Phys.*, 2014, **16**, 856–871.
8 I. Powis, in *Adv. Chem. Phys.*, ed. J. C. Light, Wiley, New York, 2008, vol. 138, pp. 267–329.
9 V. Ulrich, S. Barth, S. Joshi, U. Hergenhahn, E. A. Mikajlo, C. J. Harding and I. Powis, *J. Phys. Chem. A*, 2008, **112**, 3544–3549.
10 S. Daly, I. Powis, G. A. Garcia, H. Soldi-Lose and L. Nahon, *J. Chem. Phys.*, 2011, **134**, 064306.
11 C. Lux, M. Wollenhaupt, T. Bolze, Q. Q. Liang, J. Kohler, C. Sarpe and T. Baumert, *Angew. Chem., Int. Ed.*, 2012, **51**, 5001–5005.
12 C. S. Lehmann, N. B. Ram, I. Powis and M. H. M. Janssen, *J. Chem. Phys.*, 2013, **139**, 234307.
13 C. Lux, M. Wollenhaupt, C. Sarpe and T. Baumert, *ChemPhysChem*, 2015, **16**, 115–137.
14 M. M. Rafiee Fanood, I. Powis and M. H. M. Janssen, *J. Phys. Chem. A*, 2014, **118**, 11541–11546.
15 C. S. Lehmann, N. B. Ram and M. H. M. Janssen, *Rev. Sci. Instrum.*, 2012, **83**, 093103.
16 A. Vredenborg, W. G. Roeterdink and M. H. M. Janssen, *Rev. Sci. Instrum.*, 2008, **79**, 063108.
17 A. Vredenborg, C. S. Lehmann, D. Irimia, W. G. Roeterdink and M. H. M. Janssen, *ChemPhysChem*, 2011, **12**, 1459–1473.
18 G. A. Garcia, L. Nahon and I. Powis, *Int. J. Mass Spectrom.*, 2003, **225**, 261–270.
19 M. A. Smialek, M. J. Hubin-Franskin, J. Delwiche, D. Duflot, N. J. Mason, S. Vronning-Hoffmann, G. G. B. de Souza, A. M. F. Rodrigues, F. N. Rodrigues and P. Limao-Vieira, *Phys. Chem. Chem. Phys.*, 2012, **14**, 2056–2064.
20 J. R. A. Moreno, T. R. Huet and J. J. L. Gonzalez, *Struct. Chem.*, 2013, **24**, 1163–1170.
21 J. D. Watts, S. R. Gwaltney and R. J. Bartlett, *J. Chem. Phys.*, 1996, **105**, 6979–6988.
22 G. A. Garcia, L. Nahon, S. Daly and I. Powis, *Nat. Commun.*, 2013, **4**, 2132.
23 I. Powis, *J. Chem. Phys.*, 2014, **140**, 111103.